

Effects of cobalt doping on the reactivity of hausmannite for As(III) oxidation and As(V) adsorption

Shuang Zhang, Hui Li, Zhongkuan Wu, Jeffrey Post, Bruno Lanson, Yurong Liu, Biyun Hu, Mingxia Wang, Limei Zhang, Mei Hong, et al.

▶ **To cite this version:**

Shuang Zhang, Hui Li, Zhongkuan Wu, Jeffrey Post, Bruno Lanson, et al.. Effects of cobalt doping on the reactivity of hausmannite for As(III) oxidation and As(V) adsorption. Journal of Environmental Sciences, 2022, 122, pp.217-226. 10.1016/j.jes.2022.02.004 . insu-03833487

HAL Id: insu-03833487
https://insu.hal.science/insu-03833487

Submitted on 28 Oct 2022

HAL is a multi-disciplinary open access archive for the deposit and dissemination of scientific research documents, whether they are published or not. The documents may come from teaching and research institutions in France or abroad, or from public or private research centers.

L'archive ouverte pluridisciplinaire **HAL**, est destinée au dépôt et à la diffusion de documents scientifiques de niveau recherche, publiés ou non, émanant des établissements d'enseignement et de recherche français ou étrangers, des laboratoires publics ou privés.

Effects of cobalt doping on the reactivity of hausmannite for As(III) oxidation and As(V) adsorption

Shuang Zhang[1,2], Hui Li[3], Zhongkuan Wu[4], Jeffrey E. Post[5], Bruno Lanson[6], Yurong Liu[1,2], Biyun Hu[7], Mingxia Wang[1,2], Limei Zhang[1,2], Mei Hong[8], Fan Liu[1,2], Hui Yin[1,2,*]

[1]Key Laboratory of Arable Land Conservation (Middle and Lower Reaches of Yangtse River), Ministry of Agriculture and Rural affairs, College of Resources and Environment, Huazhong Agricultural University, Wuhan 430070, China. E-mail: 1048578935@qq.com

[2]State Environmental Protection Key Laboratory of Soil Health and Green Remediation, Ministry of Ecology and Environment, Huazhong Agricultural University, Wuhan 430070, China

[3]Environmental Sciences Division, Oak Ridge National Laboratory, Oak Ridge, TN 37831

[4]College of Environment, Zhejiang University of Technology, Hangzhou 310014, China

[5]Department of Mineral Sciences, NHB 119, Smithsonian Institution, Washington DC 20013-7012, USA

[6]Univ. Grenoble Alpes, Univ. Savoie Mont Blanc, CNRS, IRD, Univ. Gustave Eiffel, ISTerre, F-38000 Grenoble, France

[7]The Forestry Prospect Design Institute Of Hubei Province, Wuhan 430070, China

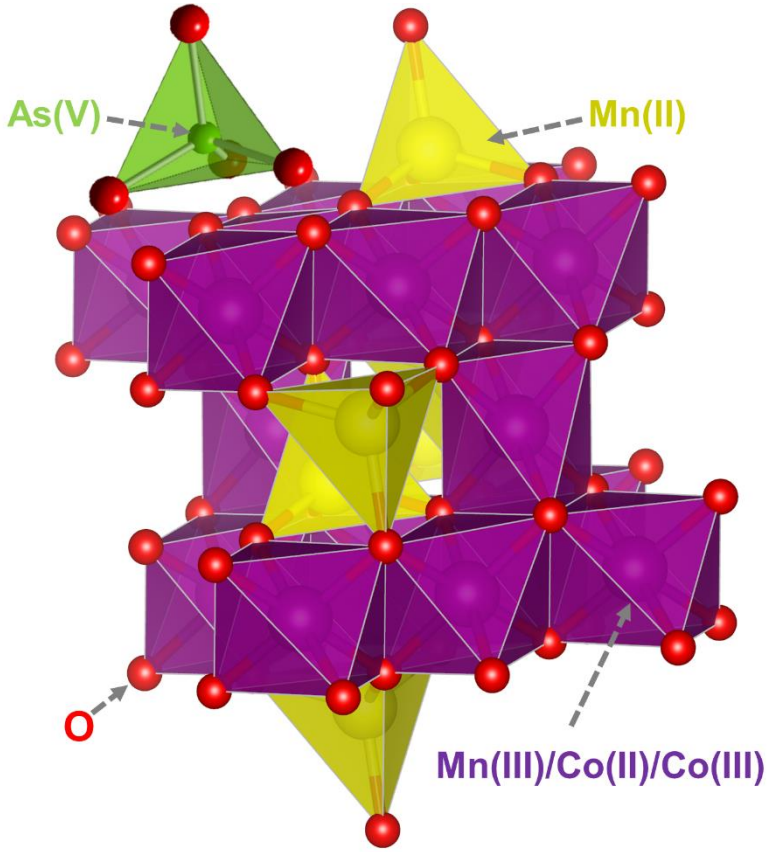
[8]College of Grassland, Resources and Environment, Inner Mongolia Agricultural University, Hohhot 010018, China

Corresponding Authors:

Tel.: +86 27 87280271. Fax: +86 27 87288618.

Email: yinhui666@mail.hzau.edu.cn (H. Yin).

Graphical Abstract:



Abstract: Hausmannite is a common low valence Mn oxide mineral, with a distorted spinel structure, in surficial sediments. Although natural Mn oxides often contain various impurities of transitional metals (TMs), few studies have addressed the effect and related mechanism of TM doping on the reactivity of hausmannite with metal pollutants. Here, the reactivity of cobalt (Co) doped hausmannite with aqueous As(III) and As(V) was studied. Co doping decreased the point of zero charge of hausmannite and its adsorption capacity for As(V). Despite a reduction of the initial As(III) oxidation rate, Co-doped hausmannite could effectively oxidize As(III) to As(V), followed by the adsorption and fixation of a large amount of As(V) on the mineral surface. Arsenic K-edge EXAFS analysis of the samples after As(V) adsorption and As(III) oxidation revealed that only As(V) was adsorbed on the mineral surface, with an average As-Mn distance of 3.25–3.30 Å, indicating the formation of bidentate binuclear complexes. These results provide new insights into the interaction mechanism between TMs and low valence Mn oxides and their effect on the geochemical behaviors of metal pollutants.

Keywords: Mn oxide; hausmannite; transition-metal; cobalt; arsenate adsorption; arsenite oxidation.

Introduction

Hausmannite, the fifth most common Mn oxide mineral in soils and sediments, is commonly present in hydrothermal and metamorphic deposits (Giovannelli et al., 2012; Peña et al., 2007). It has considerable adsorption and redox reactivity for a variety of metal pollutants (Barreto et al., 2020; Shaughnessy et al., 2003; Song et al., 2020; Wilk et al., 2005). Compared with other Mn oxides, hausmannite has a high point of zero charge (Barreto et al., 2020; Shaughnessy et al., 2003), and thus may carry a positive charge even under near-neutral pH conditions, which may greatly promote its adsorption reactivity with anionic pollutants such as arsenate ($As(V)O_4^{3-}$). Arsenate pollution has aroused great environmental concerns globally due to its high toxicity (Choong et al., 2007; Habuda-Stanic and Nujic, 2015). Adsorption by minerals such as hausmannite has been demonstrated to be an effective way to remove As(V) from wastewaters. Previous studies have shown that the adsorption capacity of hausmannite for As(V) gradually decreases with increasing pH (Barreto et al., 2020; Garcia et al., 2014). However, there have also been some reports about the pH-independent adsorption of hausmannite for As(V) (Parsons et al., 2009). The various coexisting anions (SO_4^{2-}, PO_4^{3-}, Cl^- and NO_3^-) have minor effects on As(V) adsorption (Garcia et al., 2014).

Hausmannite can also oxidize low-valence redox-sensitive elements such as As(III) and Cr(III) (Garcia et al., 2014; Weaver and Hochella Jr., 2003; Xu et al., 2017). It has been added to paddy soils to enhance arsenite oxidation and retention, thereby reducing the mobility and toxicity of soil As (Xu et al., 2017). The oxidation of As(III) by hausmannite is greatly affected by the reaction pH. It has been reported that the oxidation of As(III) is significantly more efficient with increasing pH from 7 to 12 (Feng et al., 2006). Under acidic conditions, the maximum binding of As(III) on hausmannite was observed at pH 4–5 (Feng et al., 2006; Parsons et al., 2009); however,

a reduction of As(III) adsorption with increasing pH from 2 to 6 was also reported (Garcia et al., 2014). Ionic strength (e.g., Cl^-) has little influence on As(III) adsorption (Feng et al., 2006). Low concentrations of tartaric acid promotes the oxidation of As(III), but tartaric acid at high concentrations inhibits the reaction (Feng et al., 2006). After As(III) oxidation, the changes in the average hausmannite particle sizes were minimal and could not be detected by XRD analysis (Parsons et al., 2009). In a previous study, As K-edge XANES analysis for the reaction of hausmannite and hausmannnite-magnetite with As(III) at an initial pH of 5 and a final pH of 6–7 demonstrated that all As retained on the mineral surface was As(V) (Silva et al., 2012). Raman and FTIR analysis revealed that As(V) was adsorbed on these minerals as monodentate mononuclear (MM) and bidentate mononuclear (BM) complexes (Silva et al., 2013). Recently, investigation of As(V) adsorption onto hausmannite using attenuated total reflection-Fourier transform infrared (ATR-FTIR) spectroscopy demonstrated that As(V) was adsorbed onto hausmannite surfaces as bidentate complexes at high pH during the early adsorption stage and with low surface coverage. With decreases in pH and increases in adsorption time and surface loading, more As(V) species were adsorbed as outer-sphere and/or protonated inner-sphere monodentate species (Barreto et al., 2020). As K-edge extended X-ray absorption fine structure (EXAFS) spectroscopy demonstrated that As adsorbed on hausmannite surfaces through As(V) adsorption and As(III) oxidation at pH 5 formed binuclear bidentate complexes (Parsons et al., 2009).

Mn oxide minerals in various geological settings are often enriched in various transition metals (TMs) (Baron et al., 1998). Incorporation of TMs into Mn oxides can modify their structure, physicochemical properties and reactivites with various pollutants (Song et al., 2020; Yin et al., 2012). Our previous studies investigated the effects of TMs on the reactivity of hexagonal birnessite with various pollutants. The results clearly demonstrated that TM-containing minerals, which are closer to natural analogs, tend to have much different reactivities with pollutants compared with the corresponding pristine minerals. For example, incorporation of Ni into hexagonal

birnessite greatly reduced the adsorption capacity of birnessite for heavy metals (Pb(II) or Zn(II)) by 79%–85% (Yin et al., 2012). The removal efficiencies of Cr(III) from water by Co- and Ni-containing birnessite were only 28%–55% and 67%–78% that of pure birnessite, respectively (Yin et al., 2020). As a low-valence Mn oxide, hausmannite is also capable of incorporating various substituents including Co, Ni, Fe and Al (Antao et al., 2019; Baron et al., 1998; Bordeneuve et al., 2010; Song et al., 2020). Substitution of Fe(III) for Mn(III) into the octahedral site of hausmannite decreases the Jahn-Teller distortion, increases the Curie point, and decreases the spontaneous magnetization (Baron et al., 1998). Zn doping changes the morphology of hausmannite crystallites from nanorods to a mixture of nanorods and nanoparticles, as well as increases the energy band gap (Jha et al., 2012). Pb doping greatly reduces the Mn_3O_4 particle size and increases the energy band gap, dielectric constant, and AC conductivity (Şahin et al., 2020). Doping with various TMs (Cr(III), Co(II), Ni(II), and Cu(II)) can greatly enhance the phase stability during cycling and charge-transfer behaviors of hausmannite (Dong et al., 2013). However, these studies were mainly focused on the application of TM-modified hausmannite in material sciences, and few studies have been carried out to explore the dopant effects on the reactivity of hausmannite with environmental pollutants. It has been recently reported that Ni substitution in hausmannite leads to noticeable changes in the mineral structure (e.g. lattice parameters), and enhances the acid dissolution and oxidation reactivity of hausmannite with As(III) at pH 5 (Song et al., 2020). These findings indicate that impurities may modify the structure and physicochemical properties of hausmannite and thus alter its adsorption behavior and redox reactivity with pollutants. Unlike Ni, Co is highly redox-sensitive, and the influence of Co incorporation on the reactivity and stability of hausmannite remains to be elucidated.

In this study, we investigated the effect of Co doping on the reactivity of hausmannite for the removal of As(III) and As(V) from water. The influence of environmental conditions (pH and ionic strength) on the As(V) adsorption by Co-doped hausmannite was also studied. For As(III) oxidation, changes in the concentration of

various As species were also monitored during oxidation. As K-edge EXAFS data from samples after both As(V) adsorption and As(III) oxidation were collected and analyzed to reveal the adsorption mechanisms. Our results provide new insights into the interaction mechanisms of low valence Mn oxides with TMs, and the influences of these minerals on the geochemical behaviors of heavy metal pollutants in surficial environments.

1 Materials and methods

1.1 Chemical and materials

All chemical reagents used in this study were purchased from Sinopharm Chemical Reagent Co. Ltd., China. Manganese sulfate ($MnSO_4 \cdot H_2O$; analytical grade), cobalt sulfate ($CoSO_4 \cdot 7H_2O$; analytical grade) and sodium hydroxide (NaOH; analytical grade) were used to synthesize Co-doped hausmannite. Potassium chloride (KCl; analytical grade) was used for PZC analysis. Di-sodium hydrogen arsenate ($Na_2HAsO_4 \cdot 12H_2O$; analytical grade), sodium arsenite ($NaAsO_2$; analytical grade) and sodium nitrate ($NaNO_3$; analytical grade) were used to prepare the simulated wastewater. Potassium borohydride (KBH_4; guaranteed reagent) and hydrochloric acid (HCl 32%; guaranteed reagent) were used for As(III) analysis. Potassium bromide (KBr; spectroscopically grade) was used for FTIR analysis. Deionized water (18 MΩ cm resistance) obtained from Aquapro Water Pro Ps was used to prepare stock solutions and wash the products for all experiments.

1.2 Synthesis and characterization of Co-doped hausmannite

Three Co-doped hausmannite samples with initial Co/Mn molar ratios of 0, 0.05 and 0.10 (HM, CoH5 and CoH10) were prepared using the co-precipitation method (Giovannelli et al., 2012). The phase identification and determination of the basic physicochemical properties were described in detail in a previous study (Zhang et al., 2021).

The point of zero charge (PZC) of the as-prepared samples was determined with the salt addition method (Bhowmik et al., 2016). About 20 mL of 0.01 mol/L KCl solution was added to a series of 100 mL test tubes, and the solution pH values were

adjusted to 2.0–8.0, respectively, with 0.1 mol/L HCl or 0.1 mol/L NaOH solution, and recorded as the initial pH. Then, 0.0200 g of mineral was added to each tube, and the suspension was rotated thoroughly for 48 hr. At the end of reaction, the slurry was filtered and the pH of the filtrate was recorded as pH_f. The change of pH from pH_i to pH_f (ΔpH) was plotted against pH_i; the value of pH_i at which the ΔpH was equal to zero represented the PZC of the tested solid.

1.3 As(V) adsorption experiments

Co-doped hausmannite samples (1 g) were suspended in 250 mL of 0.1 mol/L $NaNO_3$ solution for 24 hr to eliminate the effect of stirring and surface hydration, during which the pH was kept at 4.5 ± 0.05. About 10 mL of each mineral suspension was added to a 50 mL centrifuge tube, and then 0–3.2 mL of 10 mmol/L As(V) solution (pH 4.5; containing 0.1 mol/L $NaNO_3$ solution) was added, followed by the addition of 0.1 mol/L $NaNO_3$ solution to make a final reaction volume of 40 mL. These tubes were agitated mechanically in a shaker at 25 ± 2℃ for 24 hr. The ionic strength (0.01 mol/L, 0.1 mol/L and 0.2 mol/L) and reaction pH (4.5, 5.5, 6.5 and 7.5) were measured. The mixture pH was adjusted to the required value by the addition of 0.1 mol/L HNO_3 or NaOH solution during the reaction. At the end of the reaction, the suspensions were centrifuged, filtered, and the As(V) concentration in the filtrate was analyzed with the colorimetric method (Oscarson et al., 1980).

1.4 As(III) oxidation experiments

About 0.150 g of HM or CoH10 was added to 276 mL of 0.1 mol/L $NaNO_3$ solution at pH 4.50 ± 0.05 for aquotization for 24 hr. The As oxidation experiment was initiated by quick addition of 24 mL of 2.636 mmol/L $NaAsO_2$ solution (pH = 4.50 ± 0.05; with 0.1 mol/L $NaNO_3$ solution) into the mineral suspension to make a final As concentration of 15.8 mg/L. The reaction was allowed to proceed at pH 4.50 ± 0.05 for 24 hr. At certain time intervals, a 5 mL aliquot of mixture was taken and immediately filtered through a 0.22 μm membrane. At the end of the reaction, the mixture was centrifuged. The As(III) and total As (As(T)) in the filtrate were measured by atomic fluorescence spectrometry (AFS) using 1.5% HCl -1.5% KBH_4 and 5% HCl -2 % KBH_4

as the carrying fluid. The concentration of As(V) in the solution was calculated by subtracting the As(III) concentration from As(T) in the solution. The concentrations of Mn(II) and Co(II) in the filtrate were determined by AAS.

The obtained solids at the end of reaction of As(III) oxidation and As(V) adsorption were washed thoroughly, and the wet pastes were covered with Kapton tape for XAFS analysis.

1.5 X-ray absorption fine structure (XAFS) spectroscopy

The XAFS data were collected on the 1W1B beamline at the Beijing Synchrotron Radiation Facility (BSRF) at room temperature (Yin et al., 2012). As K-edge XAFS data were collected in florescence mode over the energy range of 11635 to 12882 eV. Reduction and analysis of XAFS data were performed using Athena and Artemis from the Ifeffit software package (Ravel and Newville, 2006). As K-edge spectra were background-subtracted using the following parameters: E_0 = 11872 eV, *Rbkg* = 1.0 Å and k-weight = 2. Structural parameters (bond length (*R*), coordination number (*CN*), and Debye-Waller factor (σ^2)) for As were obtained by fitting the k^3-weighted EXAFS data to the standard EXAFS equation (Kelly et al., 2008). Phase and amplitude functions for single- and multi-scattering paths were calculated using Feff7.0 (Rehr et al., 1992). As K-edge EXAFS data were fitted in an R space of 1 to 4 Å over a k range of 3.4–12.4 $Å^{-1}$, using several single scattering paths and one multiple scattering path calculated based on the structure of $MnAsO_4$ (ICSD 73489). An amplitude reduction factor (S_0^2) of 0.978 for As was determined by fitting the As–O shell of Na_3AsO_4 in an R range of 1–2 Å. In all fits, the number of independent variables was much smaller than that of independent data points allowed. During Fourier transformation and EXAFS data fitting, a Hanning window was used.

2 Results

2.1 Basic physicochemical properties of Co-doped hausmannite

The structure and basic physicochemical properties of the Co-doped hausmannite samples were described in detail in our previous paper (Zhang et al., 2021) and summarized in **Table 1**. With increasing doping amounts of Co, the Mn content

gradually decreased. The final Co/Mn molar ratios in these samples were 0.05 (CoH5) and 0.11 (CoH10). The Co-doped hausmannites consisted of cubic nanocrystals, and the TEM images showed that the average particle size was 85 ± 18, 131 ± 27 and 103 ± 28 nm for HM, CoH5 and CoH10, respectively (**Appendix A Fig. S1**). The increase in particle sizes of CoH5 and CoH10 resulted in slight decreases in specific surface area from 12.4 m^2/g to 11.7–11.8 m^2/g. The PZC of HM was 7.04 ± 0.03 (**Appendix A Fig. S2**), and Co doping resulted in a slight decrease in PZC, consistent with reports that the PZC of Co compounds, including CoOOH and Co_2O_3, is 6.9 and 6.2, respectively (Kosmulski, 2009).

2.2 As(V) adsorption at the mineral-water interface

The effects of ionic strength and pH on the As(V) adsorption by the Co-doped hausmannite samples were systematically analyzed (**Fig. 1a**). With increasing $NaNO_3$ concentration from 0.01 mol/L to 0.2 mol/L, the As(V) adsorption density on HM remained almost constant at a given pH. By contrast, at a given ionic strength, pH greatly affected As(V) adsorption; as pH increased from 4.5 to 7.5, the As(V) adsorption density decreased from 5.29–5.61 mg/g to 0.13–0.19 mg/g (**Fig. 1a**). Similar results have been reported for As(V) and Cr(VI) adsorption on hausmannite at pH 2–8 (Barreto et al., 2020; Cantu et al., 2014; Garcia et al., 2014). This strong pH dependency of As(V) adsorption can be mainly ascribed to the reduced competition between As(V) and OH^- for surface sites at lower pH. According to the dissociation constants of H_3AsO_4 (pK_1 = 2.26, pK_2 = 6.76 and pK_3 = 11.29) (Lide and Haynes, 2010), As(V) mainly exists as anionic As species of $H_2AsO_4^-$ and $HAsO_4^{2-}$ in the tested pH range.

Adsorption isotherm experiments were conducted with initial As(V) concentrations of 0–60 mg/L (**Fig. 1b**). With increasing As(V) concentration, the As(V) adsorption first showed a sharp increase, and then leveled off at high As(V)concentrations. Co-doped hausmannite samples showed similar As(V) adsorption behaviors as HM; however, the As(V) removal by Co-doped samples from the solution gradually decreased with increasing Co doping level. Analyses of the isotherm adsorption data with the Langmuir and Freundlich adsorption models (**Fig. 1b**

and Appendix A Table S1) revealed that the Freundlich model significantly better fit the data than did the Langmuir model, suggesting that the active sites on the Co-doped samples are energetically heterogeneous. The k values obtained from the Freundlich model fitting indicated that the adsorption capacity of CoH10 for As(V) was about 36% lower than that of HM. This decrease in adsorption capacity may be ascribed to the decrease in PZC of Co-doped hausmannite, indicating that the decrease in positive charge is unfavorable for As(V) adsorption.

2.3 As(III) oxidation at the mineral-water interface

In the pH range of most natural waters, soils and sediments, As(III) usually exists as neutral H_3AsO_3 molecules, while As(V) usually exists in the forms of $H_2AsO_3^-$ and $HAsO_3^{2-}$ anions, which can be readily adsorbed onto the mineral surfaces. Therefore, As(III) has higher mobility and ecological toxicity than As(V). We, therefore, investigated the effect of Co doping on the interaction between hausmannite and As(III). The As oxidation experiments were conducted by the reaction of the solutions containing As(III) (15.8 mg/L) and HM (0.5 g/L) in air atmosphere at 25℃ and pH 4.5. The control experiment was also conducted under the same conditions, but under N_2, to investigate the effect of O_2 on the oxidation of As(III) to As(V) (**Appendix A Fig. S3**). In both atmospheres, the As(V) concentrations in the solutions were almost the same, indicating that O_2 in air has a negligible effect on As(III) oxidation by hausmannite.

Figures 2a, b present the plots of concentrations of various As species in the reaction systems with time. The amount of As(V) in the solution gradually increased, confirming the oxidation of As(III) by Mn(III) (Song et al., 2020; Song et al., 2021). Concurrently, As(III) in the solution was quickly depleted, which could be attributed to the oxidation of As(III) to As(V) and the adsorption of As(V) onto the mineral surface. The adsorption of both As(III) and As(V), generated by oxidation, contributed to the decrease in total As in the solution. For all the reactions, the concentrations of the As species approached equilibrium after 2 hr, which may be ascribed to the effect of surface passivation. Hausmannite has a high PZC, and thus its surface is positively charged at

pH 4.5 and can adsorb large amounts of As species, which eventually leads to the blocking of the active sites. At equilibrium, As adsorption and fixation on the mineral surface were the dominant process, and the As in the solution was mostly As(V). At the end of the reaction, the amount of As adsorbed and fixed on the mineral surface was 13.24 ± 0.66 mg/L for HM and 12.16 ± 0.70 mg/L for CoH10. The total concentration of As(V) in the solution and adsorbed/fixed on the mineral surface was almost the same for HM (15.58 ± 0.71 mg/L) and CoH10 (15.43 ± 0.75 mg/L), which accounted for 99 ± 4% and 98 ± 5% of the initial amount of added As(III), respectively. The oxidation capacities of HM and CoH10 for As(III) were 416 ± 19 mmol/kg and 412 ± 20 mmol/kg, respectively.

The As(III) oxidation rate was quantified by fitting the reaction data over 0–0.5 hr using a pseudo-first order kinetic model (**Fig. 2c**). The As(III) oxidation rate constants for HM and CoH10 were 0.0504 ± 0.0011 min^{-1} and 0.0219 ± 0.0012 min^{-1}, respectively. The differences in oxidation rate between the samples may be ascribed to several reasons. Firstly, TEM analysis showed that CoH10 had a larger particle size and therefore a lower active site density than HM (Zhang et al., 2009). Another possible reason is that the crystal field stabilization energy (CFSE) of low-spin Co(III) ion (534.2 kJ/mol) is higher than that of Mn(III) (150.8 kJ/mol), and thus the Co(III)-O bond has higher binding energy than the Mn(III)/Mn(II)-O bond, resulting in greater activation energy at these Co(III) sites, and correspondingly a slower reaction rate (Yin et al., 2011).

During the As(III) oxidation by these Co-doped samples under the experimental conditions, large amounts of Mn(II) and Co(II) were released. In the CoH10 mineral suspension obtained by the addition of 0.1 M $NaNO_3$ solution to reach a final solid-to-liquid ratio of 0.5 g/L and equilibrated at pH 4.5 for 24 hr, the concentrations of Mn(II) and Co(II) were 148 ± 0.1 mg/L and 19 ± 0.03 mg/L, respectively. After the addition of As(III), the release of Mn(II) and Co(II) was only slightly increased. The highest Mn(II) and Co(II) concentration was measured as ~160 mg/L and ~21 mg/L, respectively (**Fig. 2d**).

2.4 Mechanism for the binding of As on mineral surface

2.4.1 FTIR analysis of HM before and after As(III) oxidation

In order to determine the mechanism for the binding of As on the hausmannite surface, FTIR analysis was conducted on a typical sample after reaction with As(III) (HM_0.8As(III)) (**Fig. 3**). Compared with the spectrum of pristine HM, the spectrum of HM_0.8 As(III) clearly showed an additional peak at 750 cm^{-1}. This peak matched that reported for an in-situ ATR-FTIR analysis of As(III) reaction with hausmannite (Song et al., 2020; Song et al., 2021), which corresponds to the vibration of As(V)-O-Mn(III), indicating the formation of As(V) bidentate binuclear surface complexes on the mineral surface.

2.4.2 Arsenic K-edge XAFS analysis

The As K-edge XAFS spectra of HM and CoH10 after As(V) adsorption and As(III) oxidation were analyzed to investigate the surface As valence and local bonding structure on the mineral surface. A comparison of the As K-edge XANES spectra of the samples with those of As(III) and As(V) standards (As_2O_3 and Na_3AsO_4) demonstrated that only As(V) was bound to HM and CoH10 surfaces during As(V) adsorption and As(III) oxidation experiments (**Fig. 4**). This result is consistent with the XANES, Raman and infrared analyses of hausmannite after As(III) oxidation in previous studies, which demonstrated that As was adsorbed in the form of As(V) (Silva et al., 2013; Silva et al., 2012).

The EXAFS spectra for all of the As-loaded hausmannite samples showed similar oscillations, indicating that they had similar local atomic structures. However, these spectra were different from those of Na_3AsO_4 (**Fig. 5A**), which was especially obvious in the corresponding FTs (**Fig. 5B**). Each of the FTs showed a major peak at $R+\Delta R$ ~ 1.3 Å, which can be assigned to the As-O shell in the [AsO_4] unit. Additionally, there was a peak at $R+\Delta R$ ~ 2.9 Å in As-loaded hausmannite, but this peak was absent in the spectrum of Na_3AsO_4, suggesting that As forms inner-sphere complexes on the mineral surface.

Fittings of the As K-edge EXAFS spectra for the hausmannite samples yielded As-

O distances ranging from 1.68–1.72 Å (**Fig. 5** and **Table 2**). These distances are identical to the previously reported As(V)-O distances for As(V) associated with Mn-oxides and Fe-oxides (Foster et al., 2003; Lafferty et al., 2010; Manning et al., 2002; Zhang et al., 2014), but shorter than the As(III)-O distance (1.75–1.77 Å) for $NaAsO_2$ or As(III) adsorbed on FeOOH (Zhang et al., 2014). This is consistent with the XANES results showing that As was adsorbed on the mineral surface in the form of As(V). Only a single As-Mn distance of 3.25–3.30 Å is needed to fit the R+ΔR ~ 2.9 Å peak.

In a previous study of As(V) adsorption on the birnessite surface, bidentate-mononuclear (BM, *R* ~2.7 Å), bidentate-binuclear (BB, *R* ~3.1–3.2 Å) and monodentate-mononuclear (MM, *R* ~3.4–3.5 Å) complexes were identified (Lafferty et al., 2010). However, the analysis of BM complexes revealed that As-O multiple scattering may also contribute to the *R* ~ 2.7 Å peak (Sherman and Randall, 2003). In the present study, an As-O multiple scattering path was added for the fitting and no BM complex was found, which is consistent with a previous finding about the binding mechanism of As on birnessite in the presence of Fe(II) (Wu et al., 2018). During the As(III) oxidation by birnessite in a stirred-flow system, the Mn(III) content gradually increased. The binding of As(V) to Mn(III) sites probably contributed to the observed increase in BB As-Mn distance from 3.12–3.13 Å to 3.19–3.23 Å, and the decrease in MM As-Mn distance from 3.42–3.47 Å to 3.34 Å (Lafferty et al., 2010). The As(V) retained on the Ni-doped hausmannite surface during As(V) adsorption and As(III) oxidation resulted in an As-Mn distance of 3.28–3.35 Å, as determined by EXAFS fitting, which could be assigned to the formation of BB complex on Mn(III) sites (Song et al., 2020). A quantum chemical study of As(V) adsorption on Mn(III) sites in Mn oxides also indicated an As-Mn distance of 3.29–3.47 Å for BB configuration (Zhu et al., 2009). Hence, the observed As-Mn distance on Co-doped hausmannite surface could be reasonably assigned to the formation of BB complexes.

3 Discussion

3.1 As(V) adsorption mechanism

Among various Mn oxides, hausmannite has a relatively high adsorption capacity

for certain anions (Li and Jaisi, 2015). Our experiments of As(V) adsorption onto Co-doped hausmannite demonstrated that pH has a great impact on As(V) adsorption, but ionic strength has almost no effect at pH ranging from 4.5 to 7.5 (**Fig. 1a**). However, other studies suggested that the binding of As(V) onto hausmannite at pH 3 is suppressed by the presence of NO_3^- at concentrations > 3 ppm (Garcia et al., 2014), possibly because a lower pH such as pH 3 can enhance the dissolution of the mineral compared with a high pH (Luo et al., 2018).

For As(V)-adsorbed hausmannite, no As(III) was detected on the mineral surface by As K-edge XANES analysis, suggesting that no As(V) reduction occurred during adsorption under the experimental conditions in this study, which is the same as observed for As(V) adsorption on Ni-doped hausmannite (Song et al., 2020). However, in a previous study, Cr K-edge XANES analysis of Cr(VI) adsorbed on hausmannite at pH 2, 4 and 6 for 1 hr demonstrated that Cr(VI) was reduced to Cr(III), owing to the electron transfer from Mn(II) to Cr(VI) (Hernandez, 2010). This difference between As(V) and Cr(VI) adsorption behaviors on hausmannite may be attributed to the lower standard reduction potential of $H_3AsO_4/HAsO_2$ ($E^0 = 0.56$ V) relative to that of $HCrO_4^-$ /Cr(III) ($E^0 = 1.35$ V) (Lide and Haynes, 2010). Additionally, the reduction of Cr(VI) on the mineral surface may also be related to the interaction with the X-ray beam irradiation during the analysis, as in the reduction of Np(V) by the X-ray beam during XAFS analysis of Np(V) adsorption on hausmannite (Wilk et al., 2005).

Furthermore, the As K-edge EXAFS analysis demonstrated an As-Mn distance of 3.25–3.26 Å for As(V) adsorbed on the Co-doped hausmannite surface, which corresponds to the BB inner sphere complex. Raman and IR analysis of As(V)-loaded hausmannite showed that the anions were adsorbed as both monodentate- and bidentate-mononuclear complexes at pH 5 (Silva et al., 2013). Recently, an ATR-FTIR study of As(V) adsorption onto hausmannite demonstrated that low pH and high As(V) surface loading are favorable for the formation of outer-sphere or hydrogen-bonded surface complexes and inner-sphere monodentate species on mineral surfaces, while high pH and low surface loading are conducive to the formation of bidentate complexes (Barreto

et al., 2020). Another ATR-FTIR study suggested that many types of complexes, such as bidentate, monodentate, binuclear, and mononuclear moieties as well as their protonated forms, are all possibly formed on the mineral surface (Song et al., 2020). However, this is different from the EXAFS results, which indicated that the As(V) adsorbed on the mineral surface forms BB complexes (Song et al., 2020). Our EXAFS results confirm the formation of BB complexes. The inconsistency in the results of EXAFS and ATR-FTIR can be mainly ascribed to the fact that EXAFS detects the average overall information but in-situ ATR-FTIR acquires information from the surface and is more sensitive to the effects of protonation. Thus, the combination of EXAFS and in-situ ATR-FTIR is needed in future studies of interface reactions.

3.2 As(III) oxidation mechanism

Our results showed that Co-doped hausmannite has high oxidation capacity for As(III), and a large part of the generated As(V) is adsorbed on the mineral surface. Furthermore, the solution pH increased during the reaction. For example, the final pH in the CoH10 system increased to ~5.2, indicating the consumption of H^+ during the reaction (Feng et al., 2006; Silva et al., 2012).

In hausmannite, structural Mn(III) is responsible for As(III) oxidation according to the following equation:

$$2Mn(III) + As(III) = 2Mn(II) + As(V)$$

According to the equation, 2 mol of Mn(II) will be released into the solution when 1 mol of As(III) is oxidized. In previous studies, for the As(III) oxidation by hausmannite doped with 0, 1 wt.% and 2.8 wt.% Co, the Mn(II): As(V) ratios were determined to be 1.5:1, 1.7:1 and 2.0:1, respectively, which are also consistent with the results obtained for Ni-doped hausmannite (Song et al., 2020; Song et al., 2021). In the present study, before the addition of As(III), the mineral was partially dissolved, resulting in the release of 45% of the total Mn and ~57% of the total Co in CoH10 during equilibration at pH 4.5 for 24 hr. During As(III) oxidation, additional ~12 mg/L of Mn(II) and ~2 mg/L of Co(II) were released. The molar ratio of Mn(II) in the solution to total As(V) produced (including both As(V) in the solution and that adsorbed/fixed

on mineral surface) was estimated to be 1:1. The low Mn(II) concentration in the solution might be due to the re-adsorption on the As(V)-loaded mineral surface. In a previous study, less than 25% of total As was adsorbed on mineral surface (Song et al., 2020), while in the present study, 77 ± 4% of total As was adsorbed and fixed on the mineral surface in the form of As(V) (**Fig. 2**). At pH 4.5, As(V) exists predominantly in the form of $H_2AsO_4^-$ (Lide and Haynes, 2010). The retention of a large amount of anions on the mineral surface would neutralize the positive charge and make the zeta potential (ζ) more negative, which is more favorable for the re-adsorption of Mn(II) and Co(II).

Our As K-edge XAFS analysis of the As-loaded samples after As(III) oxidation showed that As was adsorbed on the mineral surface as As(V) by forming the BB complexes with the nearest As-Mn distance of 3.28–3.30 Å, which is consistent with previous studies (Song et al., 2020). These As species were relatively stable on the mineral surface, and the amount of As adsorbed and fixed on the mineral surface was almost constant after reaching reaction equilibrium (**Fig. 2**). All these results suggest that hausmannite may greatly affect the geochemical behaviors of As(III), by oxidation of As(III) to As(V), and by adsorption of As(V) on the mineral surface.

In fact, hausmannite nanomaterials have been used to remediate As(III)-polluted soils and sediments. For example, hausmannite was added to two paddy soils to enhance arsenite oxidation, leading to a decrease in As concentration in rice grains and straw (Xu et al., 2017). In natural environments, Mn oxides may contain significant amounts of metal impurities. The present study revealed that although incorporation of Co into hausmannite decreased the initial As(III) oxidation rate, the overall oxidation capacities of the various doped samples were similar. Therefore, natural hausmannite may also be highly oxidizing towards low valence redox-sensitive trace elements. However, it is necessary to continue to study reactions of hausmannite with these elements in the presence of coexisting ions, organic molecules and humic substances.

4 Conclusions

After Co doping, hausmannite showed a decrease in PZC and high reactivity for

As(III) oxidation and As(V) adsorption. Ionic strength had no effect on the adsorption of As(V) onto the mineral surface, while an increase in the reaction pH from 4.5 to 7.5 gradually decreased the adsorption capacity. The As(V) adsorption capacity gradually decreased with increasing Co doping level. Co-doped hausmannite has high oxidation activities for As(III), and most of the generated As(V) is adsorbed on the mineral surface. Although Co doping decreased the initial oxidation rate, the overall oxidation capacity of the Co-doped hausmannite was comparable to that of pristine hausmannite. The As species in hausmannite after both As(V) adsorption and As(III) oxidation probably form bidentate binuclear complexes with the nearest As-Mn distance of 3.25–3.30 Å. These results suggest that natural hausmannite may play an important role in mediating the geochemical cycling of As in surficial environments.

Acknowledgments

The authors gratefully thank the Key science and technology projects of Inner Mongolia autonomous region (2019ZD001), the National Natural Science Foundations of China (Nos.42077015, 41771267 and 41877030), the National Key Research and Development Program of China (No. 2016YFD0800403), and the Fundamental Research Funds for the Central Universities (Grant 103-510320036) for the financial support.

Appendix A. Supplementary data

Supplementary data associated with this article can be found in the online version at xxxxxx.

References

Antao, S.M., Cruickshank, L.A., Hazrah, K.S., 2019. Structural trends and solid-solutions based on the crystal chemistry of two hausmannite (Mn_3O_4) samples from the Kalahari Manganese Field. Minerals 9:343.

Baron, V., Gutzmer, J., Rundlof, H., Tellgren, R., 1998. The influence of iron

490 substitution on the magnetic properties of hausmannite, $Mn^{2+}(Fe,Mn)(_2)(^{3+})O_4$.
491 Am. Mineral. 83:786-793.
492 Barreto, M.S.C., Elzinga, E.J., Alleoni, L.R.F., 2020. Hausmannite as potential As(V)
493 filter. Macroscopic and spectroscopic study of As(V) adsorption and desorption
494 by citric acid. Environ. Pollut. 262:114196.
495 Bhowmik, K.L., Debnath, A., Nath, R.K., Das, S., Chattopadhyay, K. K., Saha, B., 2016.
496 Synthesis and characterization of mixed phase manganese ferrite and hausmannite
497 magnetic nanoparticle as potential adsorbent for methyl orange from aqueous
498 media: Artificial neural network modeling. J. Mol. Liq. 219:1010-1022.
499 Bordeneuve, H., Tenailleau, C., Guillemet-Fritsch, S., Smith, R., Suard, E., Rousset, A.,
500 2010. Structural variations and cation distributions in $Mn_{3-x}Co_xO_4$ ($0 \leq x \leq 3$)
501 dense ceramics using neutron diffraction data. . Solid State Sci. 12:379-386.
502 Cantu, Y., Remes, A., Reyna, A., Martinez, D., Villarreal, J., Ramos, H., et al., 2014.
503 Thermodynamics, kinetics, and activation energy studies of the sorption of
504 chromium(III) and chromium(VI) to a Mn_3O_4 nanomaterial. Chem. Eng. J.
505 254:374-383.
506 Choong, T.S.Y., Chuah, T.G., Robiah, Y., Koay, F.L.G., Azni, I., 2007. Arsenic toxicity,
507 health hazards and removal techniques from water: an overview. Desalination
508 217:139-166.
509 Dong, R., Ye, Q., Kuang, L., Lu, X., Zhang, Y., Zhang, X., et al., 2013. Enhanced
510 supercapacitor performance of Mn_3O_4 nanocrystals by doping transition-metal
511 ions. ACS Appl. Mater. Inter. 5:9508-9516.
512 Feng, X., Zu, Y., Tan, W., Liu, F., 2006. Arsenite oxidation by three types of manganese
513 oxides. J. Environ. Sci. 18:292-298.
514 Foster, A.L., Brown, G.E., Parks, G.A., 2003. X-ray absorption fine structure study of
515 As(V) and Se(IV) sorption complexes on hydrous Mn oxides. Geochim.
516 Cosmochim. Acta 67:1937-1953.
517 Garcia, S., Sardar, S., Maldonado, S., Garcia, V., Tamez, C., Parsons, J.G., 2014. Study
518 of As(III) and As(V) oxoanion adsorption onto single and mixed ferrite and

519 hausmannite nanomaterials. Microchem. J. 117:52-60.
520 Giovannelli, F., Autret-Lambert, C., Mathieu, C., Chartier, T., Delorme, F., Seron, A.,
521 2012. Synthesis of manganese spinel nanoparticles at room temperature by
522 coprecipitation. J. Solid State Chem. 192:109-112.
523 Habuda-Stanic, M., Nujic, M., 2015. Arsenic removal by nanoparticles: a review.
524 Environ. Sci. Pollut. Res. Int. 22:8094-8123.
525 Hernandez, J., 2010. Chromium(III/VI) binding to magnetite, hausmannite, and
526 jacobsite nanomaterials. PhD thesis. The University of Texas at EI Paso.
527 AAI1479558.
528 Jha, A., Thapa, R., Chattopadhyay, K.K., 2012. Structural transformation from Mn_3O_4
529 nanorods to nanoparticles and band gap tuning via Zn doping. Mater. Res. Bull.
530 47:813-819.
531 Kelly, S.D., Hesterberg, D., Ravel, B., 2008. Analysis of soils and minerals using X-
532 ray absorption spectroscopy, in: Ulrey A L, Drees R L (Eds.), Methods of Soil
533 Analysis, Part 5-MineralogicalMethods. Soil Science Society of America,
534 Wisconisn, pp. 387-463.
535 Kosmulski, M., 2009. pH-dependent surface charging and points of zero charge. IV.
536 Update and new approach. J. Colloid Interf. Sci. 337:439-448.
537 Lafferty, B.J., Ginder-Vogel, M., Zhu, M., Livi, K.J.T., Sparks, D.L., 2010. Arsenite
538 oxidation by a poorly crystalline manganese-oxide. 2. Results from X-ray
539 absorption spectroscopy and X-ray diffraction. Environ. Sci. Technol. 44:8467-
540 8472.
541 Li, H., Jaisi, D.P., 2015. An isotope labeling technique to investigate atom exchange
542 during phosphate sorption and desorption. Soil Sci. Soc. Am. J. 79:1340-1351.
543 Lide, D.R., Haynes, W. M., 2010. CRC Handbook of Chemistry and Physics, (90th ed.).
544 CRC Press: Florida.
545 Luo, Y., Tan, W., Suib, S.L., Qiu, G., Liu, F., 2018. Dissolution and phase
546 transformation processes of hausmannite in acidic aqueous systems under anoxic
547 conditions. Chem. Geol. 487:54-62.

548 Manning, B.A., Fendorf, S.E., Bostick, B., Suarez, D.L., 2002. Arsenic(III) oxidation
549 and Arsenic(V) adsorption reactions on synthetic birnessite. Environ. Sci. Technol.
550 36:976-981.
551 Oscarson, D.W., Huang, P.M., Liaw, W.K., 1980. The oxidation of arsenite by aquatic
552 sediments. J. Environ. Qual. 9:4:700-703.
553 Parsons, J.G., Lopez, M.L., Peralta-Videa, J.R., Gardea-Torresdey, J.L., 2009.
554 Determination of arsenic(III) and arsenic(V) binding to microwave assisted
555 hydrothermal synthetically prepared Fe_3O_4, Mn_3O_4, and $MnFe_2O_4$ nanoadsorbents.
556 Microchem. J. 91:100-106.
557 Peña, J., Duckworth, O.W., Bargar, J.R., Sposito, G., 2007. Dissolution of hausmannite
558 (Mn_3O_4) in the presence of the trihydroxamate siderophore desferrioxamine B.
559 Geochim. Cosmochim. Acta 71:5661-5671.
560 Ravel, B., Newville, M., 2006. ATHENA and ARTEMIS: Interactive graphical data
561 analysis using IFEFFIT. Phys. Scr. 115, 1007-1010.
562 Rehr, J.J., Albers, R.C., Zabinsky, S.I., 1992. High-order multiple-scattering
563 calculations of X-ray-absorption fine structure. Phys. Rev. Lett. 69:3397-3400.
564 Şahin, B., Aydin, R., Cetin, H., 2020. Tuning the morphological, structural, optical and
565 dielectric properties of hausmannite (Mn_3O_4) films by doping heavy metal lead.
566 Superlattice. Microst. 143:106546.
567 Shaughnessy, D.A., Nitsche, H., Booth, C.H., Shuh, D.K., Waychunas, G.A., Wilson,
568 R.E., et al., 2003. Molecular interfacial reactions between Pu(VI) and manganese
569 oxide minerals manganite and hausmannite. Environ. Sci. Technol. 37:3367-3374.
570 Sherman, D.M., Randall, S.R., 2003. Surface complexation of arsenic(V) to iron(III)
571 (hydr)oxides: structural mechanism from ab initio molecular geometries and
572 EXAFS spectroscopy. Geochim. Cosmochim. Acta 67:4223-4230.
573 Silva, G.C., Almeida, F.S., Dantas, M.S., Ferreira, A.M., Ciminelli, V.S., 2013. Raman
574 and IR spectroscopic investigation of As adsorbed on Mn_3O_4 magnetic composites.
575 Spectrochim Acta A 100:161-165.
576 Silva, G.C., Almeida, F.S., Ferreira, A.M., Ciminelli, V.S.T., 2012. Preparation and

577 application of a magnetic composite (Mn_3O_4/Fe_3O_4) for removal of As(III) from
578 aqueous solutions. Mat. Res. 15:403-408.
579 Song, B., Cerkez, E.B., Elzinga, E.J., Kim, B., 2020. Effects of Ni incorporation on the
580 reactivity and stability of hausmannite (Mn_3O_4): Environmental implications for
581 Mn, Ni, and As solubility and cycling. Chem. Geol. 558:119862.
582 Song, B., Cerkez, E.B., Elzinga, E..J, Kim, B., 2021. Effects of structural cobalt on the
583 stability and reactivity of hausmannite and manganite: Cobalt coordination
584 chemistry and arsenite oxidation. Chem. Geol.:120453.
585 Weaver, R.M., Hochella, M.F., 2003. The reactivity of seven Mn-oxides with Cr^{3+}_{aq}: A
586 comparative analysis of a complex, environmentally important redox reaction. Am.
587 Mineral. 88:2016-2027.
588 Wilk, P.A., Shaughnessy, D.A., Wilson, R.E., Nitsche, H., 2005. Interfacial interactions
589 between Np(V) and manganese oxide minerals manganite and hausmannite.
590 Environ. Sci. Technol. 39:2608-2615.
591 Wu, Y., Kukkadapu, R.K., Livi, K.J.T., Xu, W.Q., Li, W., Sparks, D.L., 2018. Iron and
592 arsenic speciation during As(III) oxidation by manganese oxides in the presence
593 of Fe(II): Molecular-level characterization using XAFS, Mossbauer, and TEM
594 Analysis. Acs Earth Space Chem. 2:256-268.
595 Xu, X., Chen, C., Wang, P., Kretzschmar, R., Zhao, F.J., 2017. Control of arsenic
596 mobilization in paddy soils by manganese and iron oxides. Environ. Pollut.
597 231:37-47.
598 Yin, H., Feng, X.H., Qiu, G.H., Tan, W.F., Liu, F., 2011. Characterization of Co-doped
599 birnessites and application for removal of lead and arsenite. J. Hazard. Mater.
600 188:341-349.
601 Yin, H., Sun, J., Yan, X., Yang, X., Feng, X., Tan, W.,et al., 2020. Effects of Co(II) ion
602 exchange, Ni(II)- and V(V)-doping on the transformation behaviors of Cr(III) on
603 hexagonal turbostratic birnessite-water interfaces. Environ. Pollut. 256:113462.
604 Yin, H., Tan, W.F., Zheng, L.R., Cui, H.J., Qiu, G.H., Liu, F., et al., 2012.
605 Characterization of Ni-rich hexagonal birnessite and its geochemical effects on

aqueous Pb^{2+}/Zn^{2+} and As(III). Geochim. Cosmochim. Acta 93:47-62.

Zhang, G., Liu, F., Liu, H., Qu, J., Liu, R., 2014. Respective role of Fe and Mn oxide contents for arsenic sorption in iron and manganese binary oxide: An X-ray absorption spectroscopy investigation. Environ. Sci. Technol. 48:10316-10322.

Zhang, H.Z., Chen, B., Banfield, J.F., 2009. The size dependence of the surface free energy of titania nanocrystals. Phys. Chem. Chem. Phys. 11:2553-2558.

Zhang, S., Li, H., Wu, Z., Post, J.E., Lanson, B., Elzinga, E.J., et al., 2021. Effects of Co doping on the structure and physicochemical properties of hausmannite (Mn_3O_4) and its transformation during aging. Chem. Geol. 582:120448.

Zhu, M., Paul, K.W., Kubicki, J.D., Sparks, D.L., 2009. Quantum chemical study of Arsenic(III, V) adsorption on Mn-oxides: Implications for Arsenic(III) oxidation. Environ. Sci. Technol. 43:6655-6661.

635

636

637

638

639

640 **List of tables**

641 **Table 1** Chemical composition, specific surface area (SSA) and point of zero charge

642 (PZC) of Co-doped hausmannite samples.

Sample	Element content (wt%)		Co/Mn	SSA	PZC
	Mn	Co	at. %	(m^2/g)	
HM	70.92(1)	0	0	12.4 ± 0.1	7.04(3)
CoH5	69.63(32)	3.52(5)	5	11.7 ± 0.2	6.92(1)
CoH10	65.93(116)	6.70(11)	11	11.8 ± 0.1	6.86(4)

643

644 **Table 2.** Structural parameters obtained from the fitting of As K-edge EXAFS for

645 typical samples after As(V) adsorption and As(III) oxidation.

Sample	shell	CN	R (Å)	σ^2	ΔE (eV)	R factor
HM_0.05As(V)	As-O	4.9(6)	1.695(7)	0.0025(9)	8.3(20)	0.0282
	As-Mn	0.7(9)	3.295(26)	0.0016(67)		
HM_0.4As(V)	As-O	4.9(6)	1.686(7)	0.0031(9)	6.0(22)	0.0272
	As-Mn	0.5(11)	3.263(47)	0.0040(122)		
CoH10_0.05As(V)	As-O	4.8(7)	1.688	0.0029	6.4(23)	0.0359
	As-Mn	0.9(4)	3.251(26)	0.0023(17)		
CoH10_0.4As(V)	As-O	4.1(7)	1.682	0.0014	4.9(29)	0.0459
	As-Mn	0.5	3.263(39)	0.0012(104)		
HM_0.8As(III)	As-O	3.9(5)	1.716(7)	0.0020(9)	13.4(20)	0.0388
	As-Mn	0.6(4)	3.277(39)	0.0006(19)		
CoH10_0.8As(III)	As-O	4.6(6)	1.697	0.0027	10.0(23)	0.0401

As-Mn	0.3(4)	3.297(84)	0.0017(53)

List of figures

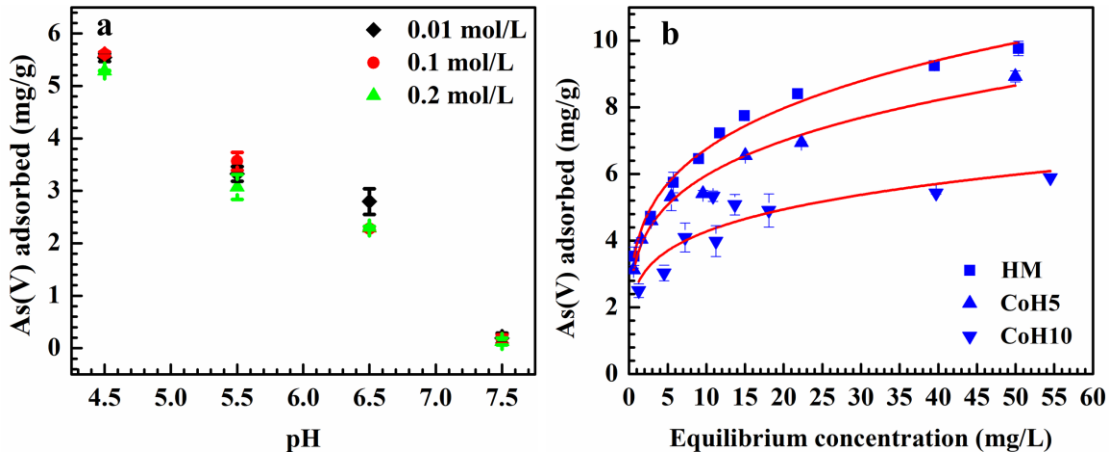


Fig. 1 (a) Effects of pH and ionic strength on As(V) adsorption on HM with an initial As(V) concentration of 7.5 mg/L and sorbent dose of 1 g/L at 25℃. (b) Adsorption isotherm curves of As(V) on Co-doped hausmannite samples, overlaid with the best fit using the Freundlich model, $Q = kC^{1/n}$, where Q is the amount of adsorbed As(V), C is the equilibrium concentration, K is the distribution coefficient, and n is a correction factor. Experimental conditions: a sorbent dose of 1g/L, ionic strength of 0.1 mol/L, and a pH of 4.5 at 25℃.

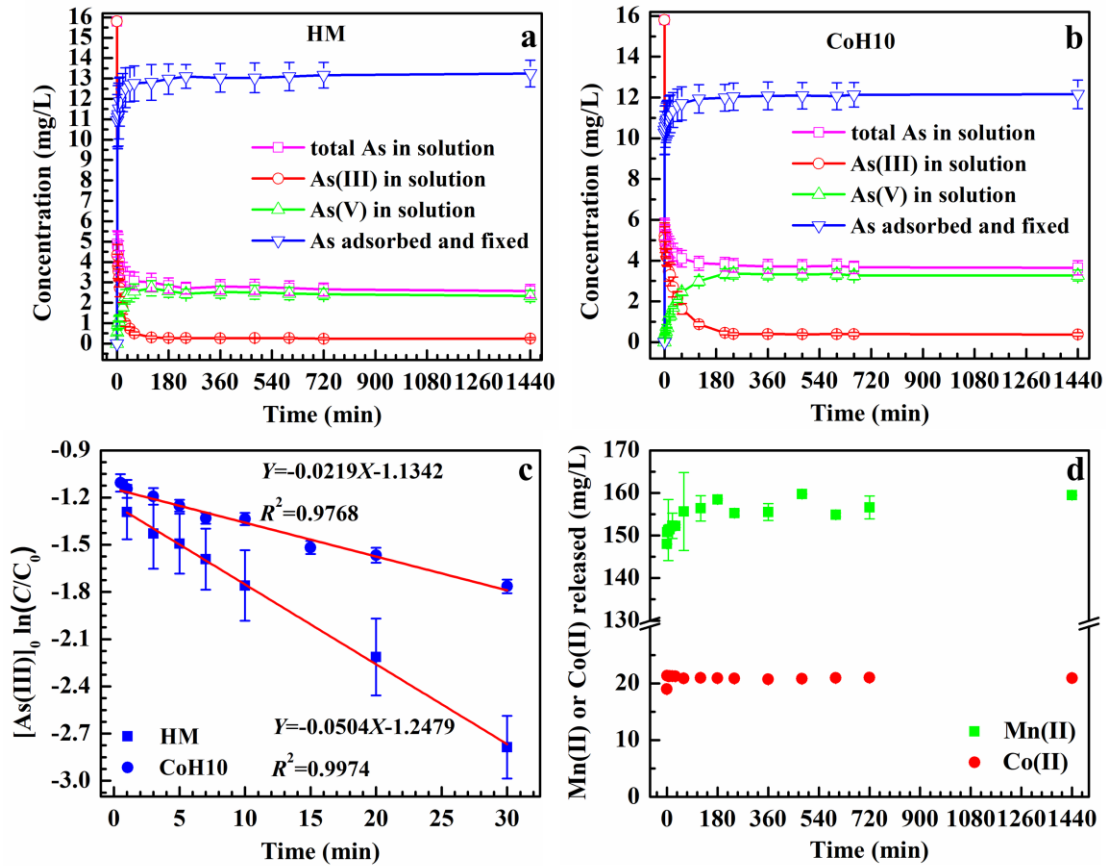


Fig. 2 Changes in the concentrations of various As species in solution and on the solid surfaces with time during the oxidation of As(III) by HM (a) and CoH10 (b), and (c) pseudo-first order kinetic modeling for As(III) depletion by HM and CoH10 at pH 4.5 during the first 30 min, and (d) release of Mn(II) or Co(II) during the As(III) oxidation by CoH10. Experimental conditions: mineral concentration = 0.5 g/L, $[As(III)]_0$ = 15.8 mg/L and $[NaNO_3]$ = 0.1 mol/L.

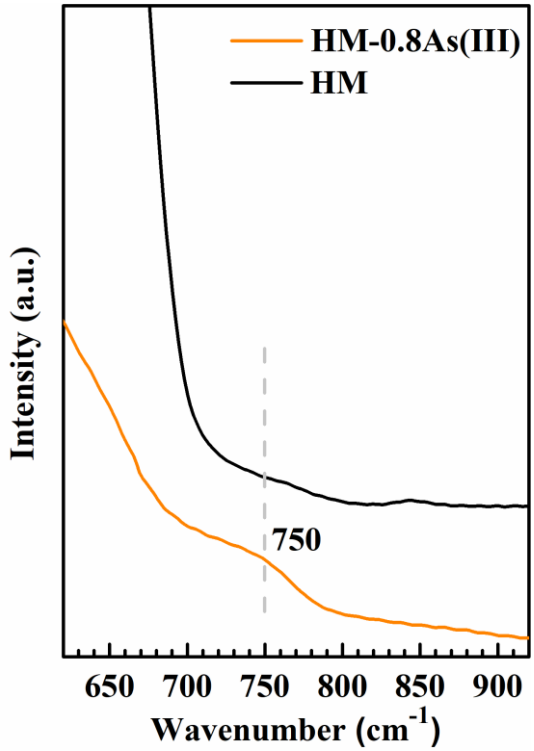


Fig. 3 FTIR spectra of pristine HM and that after reaction with As(III).

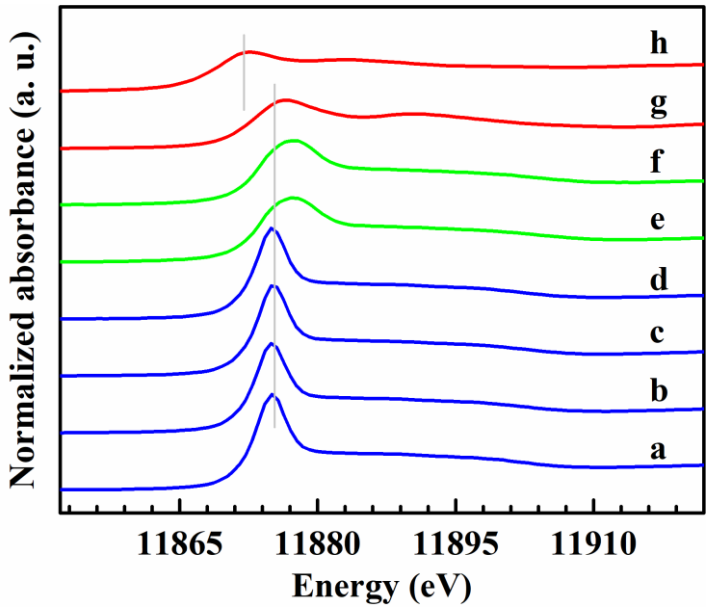
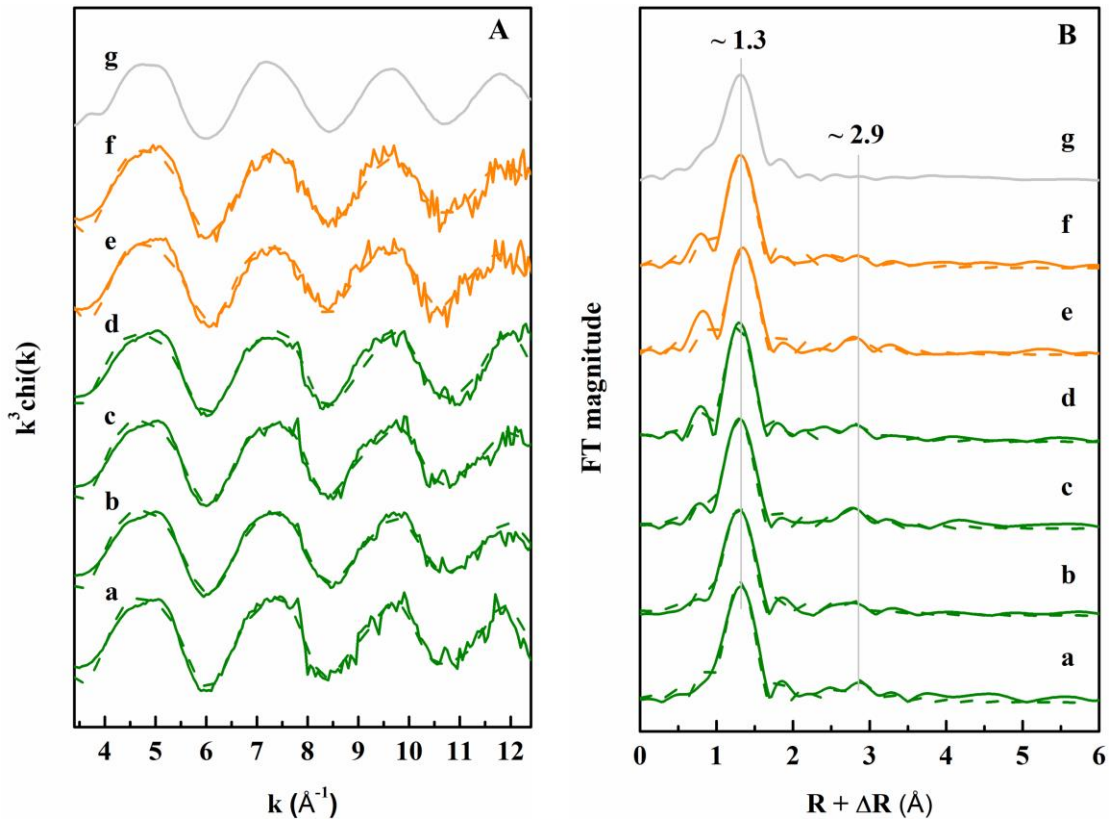


Fig. 4 Normalized As K-edge XANES spectra of reference samples (As_2O_3 and Na_3AsO_4), and HM and CoH10 after As(V) adsorption ($[As(V)]_0$ = 0.05 and 0.40 mmol/L) and As(III) oxidation ($[As(III)]_0$ = 0.8 mmol/L). (a) HM_0.05As(V), (b) HM_0.40As(V), (c) CoH10_0.05As(V), (d) CoH10_0.40As(V), (e) HM_0.80As(III), (f) CoH10_0.80As(III), (g) Na_3AsO_4 and (h) As_2O_3.



689

690 **Fig. 5** (A) As K-edge EXAFS and (B) the corresponding Fourier transformed spectra
691 (FTs) of HM and CoH10 after As(V) adsorption ($[As(V)]_0$ = 0.05 and 0.4 mmol/L) and
692 As(III) oxidation ($[As(III)]_0$ = 0.8 mmol/L). The lines are experimental data, and dashed
693 lines are the best fits.
694 (a) HM_0.05As(V), (b) HM_0.4As(V), (c) CoH10_0.05As(V), (d) CoH10_0.4As(V),
695 (e) HM_0.8As(III), (f) CoH10_0.8As(III) and (g) Na_3AsO_4

Effects of cobalt doping on the reactivity of hausmannite for As(III) oxidation and As(V) adsorption

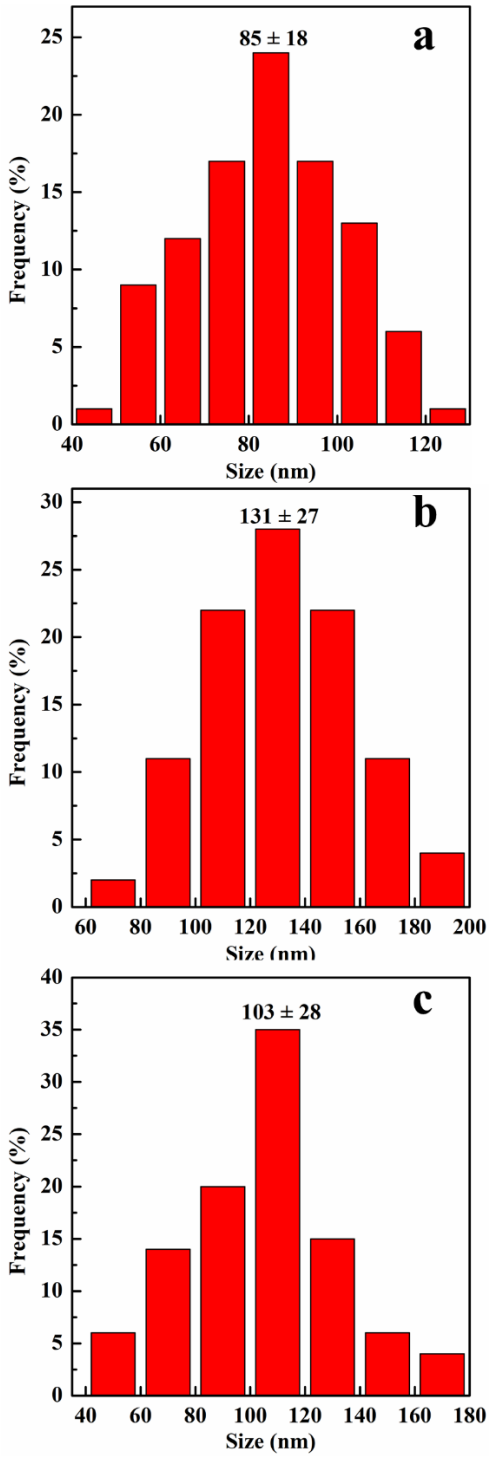


Fig. S1 Size distribution histograms of Co-doped hausmannite crystals. (a) HM, (b) CoH5, and (a) CoH10. The particle size is a statically average value by analyzing 100 crystals for each sample.

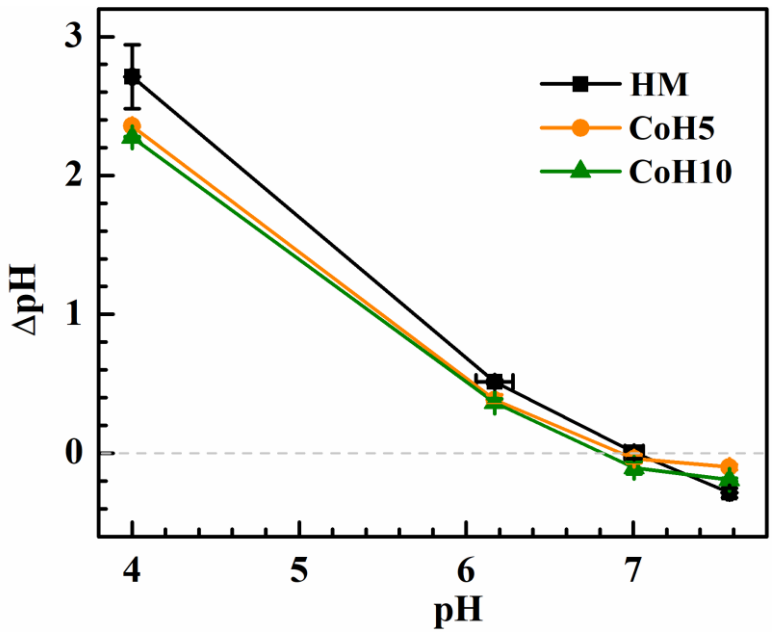


Fig. S2 The point of zero charge of Co-doped hausmannite samples.

Table S1. Fitting results of the isothermal curves for As(V) adsorption onto Co-doped hausmannite samples.

Sample	Langmuir			Freundlich		
	Q_e/(mg/g)	b/(L/mg)	R^2	k	1/n	R^2
HM	9.55	0.34	0.86	3.88	0.24	0.99
CoH5	7.60	0.62	0.77	3.49	0.23	0.98
CoH10	5.82	0.33	0.85	2.48	0.22	0.91

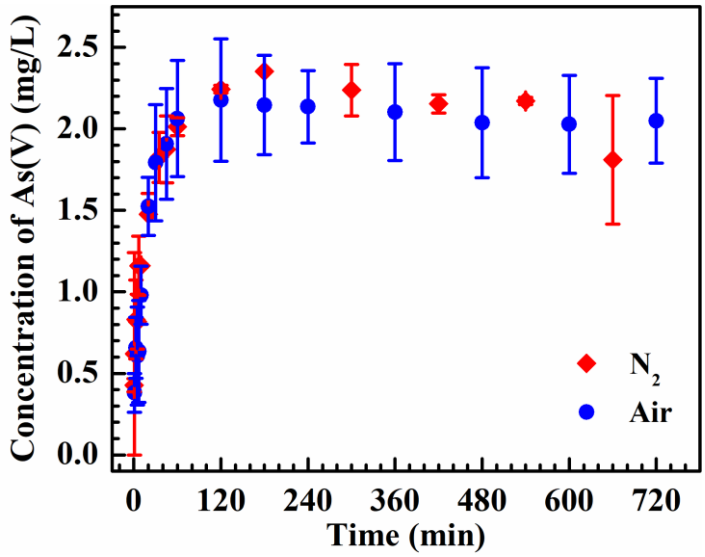


Fig. S3 Concentration of As(V) in solution during As(III) oxidation by HM under N_2 or air condition. Experiment conditions: pH=4.5, initial As(III) concentration = 15 mg/L, sorbent dose = 0.5 g/L, and ionic strength = 0.1 M $NaNO_3$ solution.